Systematic Study of the Potential Energy Surface for the Base-Induced Elimination Reaction of Fluoride Ion with Ethyl Fluoride Using Density Functional Theory

Grant N. Merrill,[‡] Scott Gronert,*[,†] and Steven R. Kass*[,‡]

Department of Chemistry and Biochemistry, San Francisco State University, San Francisco, California 94132, and the Department of Chemistry, University of Minnesota, Minneapolis, Minnesota 55455

Received: August 2, 1996; In Final Form: November 1, 1996[⊗]

The potential energy surface for the reaction between fluoride ion and ethyl fluoride was explored using density functional theory and a high-level *ab initio* procedure (G2+). A wide variety of functionals and basis sets were systematically examined. Four reactions with known thermochemistry were used as benchmarks, and while the experimental results could be reproduced, no single functional or class of functionals consistently outperformed the others. Transition structures and an ion−molecule complex, $F^-\cdot\cdot CH_3CH_2F$, are discussed. The DFT barriers are consistently smaller and looser than those obtained with high-level *ab initio* calculations. Moreover, the anti elimination transition state is unusually sensitive to the choice of functional and basis set; in many cases the transition structure does not appear to exist on the potential energy surface. The origin of this problem may reside in the large charge inhomogeneities characteristic of transition states and/or an inadequate description of the exchange interaction. This shortcoming, clearly, demands a great deal more attention.

Introduction

α,β-Elimination reactions are fundamental transformations which have been the subject of numerous experimental and theoretical investigations.[1−3] A thorough understanding of these reactions poses a formidable challenge due to the inherent complexity of the potential energy surface; two σ bonds must be broken and one π bond formed during the course of the elimination. Moreover, these events may occur in a stepwise or concerted fashion, and in the case of a concerted process, questions of synchronicity often arise.

Variable transition state theory is now routinely invoked as a unifying paradigm to elucidate elimination reactions.[3] This theory holds that there is a spectrum of possible transition states (see Figure 1). It runs from an E1 limit (where loss of the leaving group leads to a stable cationic intermediate) through a central E2 transition state (with the loss of the leaving group and the proton having occurred to a roughly equal extent) to an $E1_{cb}$ limit (where proton abstraction leads to a stable anionic intermediate). For E2 eliminations a second transition-state spectrum has been proposed as a means of describing the nature of articulation between the base and the substrate. At one end of this range of transition states, the base only interacts with the β proton (E2H), while at the other end the base also interacts with the carbon site bearing the leaving group (E2C).[4] While data exist to support an E1−E2−$E1_{cb}$ spectrum, unequivocal experimental evidence has yet to be offered that would substantiate an E2H−E2C range of transition states. As such the utility of an E2H−E2C spectrum may lie as an aid in the description of computed transition state structures.

The most important elimination reactions are based-induced, and a prototypical transformation of this type is the reaction of fluoride with ethyl fluoride. This process and

$$F^- + CH_3CH_2F \rightarrow HF + CH_2{=}CH_2 + F^- \qquad (1)$$

related ones were examined by Beauchamp and co-workers in the early days of gas-phase ion−molecule reaction studies.[5] They observed an M-1 ion with several different bases (B = OH^-, MeO^-, EtO^-) and assumed that this species was the conjugate base of ethyl fluoride ($^-CH_2CH_2F$). This led them to postulate an $E1_{cb}$-like mechanism for the elimination of hydrogen fluoride. A syn pathway was also invoked based on the formation of bifluoride ion (FHF^-, B = F^-), and BHF^- in general. Subsequent *ab initio* molecular orbital calculations found that $^-CH_2CH_2F$ is not a stable species on the potential energy surface and that an E2-like mechanism is favored.[2f,g,i] These computational results, along with additional gas-phase experiments on related systems, have led to a reevaluation of the work of Beauchamp et al. It is now assumed that the putative $E1_{cb}$ intermediate is simply a cluster between fluoride and ethylene, $[CH_2{=}CH_2\cdot\cdot F]^-$. In addition, it is also known that the formation of cluster ions such as BHF^- do not provide reliable stereochemical information (i.e., BHF^- can arise from syn *and* anti pathways).[6] To complicate matters further, it has become apparent that to adequately describe the fluoride−ethyl fluoride system, high-level *ab initio* calculations that account for electron correlation are required if the thermochemistry of fluoride and fluorine-containing species are to be accurately reproduced.[7]

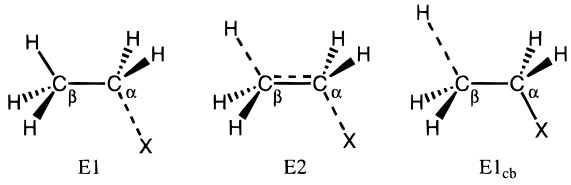

Figure 1. Schematic representation of variable transition-state (VST) theory.

Density functional theory (DFT) has experienced a renaissance in recent years through its application in the calculation of electronic structures of isolated gas-phase molecules.[8] This newfound popularity can be primarily attributed to its favorable scaling behavior when compared to more traditional *ab initio* approaches, especially those designed to recover dynamic electron correlation.[9] For example, Hartree−Fock theory (HFT)

[†] San Francisco State University.
[‡] University of Minnesota.
[⊗] Abstract published in *Advance ACS Abstracts,* December 15, 1996.

S1089-5639(96)02344-4 CCC: $14.00

scales formally as $O(N^4)$, where O is the number of occupied orbitals and N is the number of basis functions. As HFT contains no description of correlation beyond simple exchange, more elaborate, and thus costly, theories must be applied in an attempt to compensate for this deficiency. One of the more commonly used correlation methods is the perturbative approach of Møller and Plesset.[10] Second-order Møller−Plesset theory (MP2) scales formally as $O(N^5)$. More sophisticated correlation treatments (e.g., MP4 and CCSD(T)) scale even more poorly at $O(N^7)$. DFT, on the other hand, scales formally as $O(N^3)$! Clearly, for large systems in which some description of electron correlation is required, DFT holds great promise. Additionally, unlike *ab initio* techniques which attempt to describe dynamic correlation in a perturbative or configuration-interactive manner, DFT includes a correlation term *directly* in the Hamiltonian; a fact that has further contributed to its appeal within the computational community.

While the number of DFT studies has proliferated in recent years, few investigations of potential energy surfaces have been undertaken.[11] Moreover, relatively little *systematic* benchmarking of the performance of DFT has been carried out. To the best of our knowledge, no systematic studies of elimination potential energy surfaces have been published. Bickelhaupt et al. have recently reported the results of a density functional investigation on the reaction of fluoride and ethyl fluoride, but no attempt was made to assess the performance of various functionals or their basis-set dependence.[12] Their study also had a number of problems and shortcomings which we have recently described; they stem primarily from a failure to include diffuse functions (at least for heavy atoms) in the basis set and from using the Xα functional for carrying out the optimizations.[7,13] In this paper we elaborate on our initial density functional study of the fluoride−ethyl fluoride reaction system. A wide variety of functionals representing the range of those routinely used today are compared and their basis-set dependence evaluated. The results call attention to a number of potential pitfalls associated with density functional descriptions of transition states.

Experimental Section

Theory. As a number of excellent reviews of the density functional formalism, including its theoretical development and implementation, already exist in the literature,[8] only a cursory examination of the underlying theory will be made. This description will closely follow the implementation of DFT found within the popular Gaussian suite of programs. It is hoped that this brief section will offer the reader an adequate framework from within which the current results may be interpreted.

The theoretical foundation of DFT is provided by the Hohenberg−Kohn theorem which states that the ground-state electronic energy, E_{elec}, for a system is a functional of the total electronic charge density, ρ.[14] Kohn and Sham subsequently developed a series of one-electron equations, analogous to those of Hartree−Fock−Roothaan, as a practical means of implementing this seminal theorem.[15] In these equations the Kohn−Sham Hamiltonian, $\hat{H}_{KS}$, retains the kinetic, nuclear−electronic, and Coulomb terms of the Hartree−Fock Hamiltonian, $\hat{H}_{HF}$, but the exchange term is replaced with a generalized potential, V_{XC}, which is a functional of the total charge density:[16]

$$\hat{H}_{KS} = -\frac{1}{2}\nabla^2 - \sum_{A}^{\text{nuclei}} \frac{Z_A}{|r - r_A|} + \frac{1}{2}\int \frac{\rho(r_2)}{|r_1 - r_2|}\,dr + V_{XC} \qquad (2)$$

Moreover, unlike $\hat{H}_{HF}$, dynamic electron correlation is explicitly included within the potential term, V_{XC}. It is the presence of this exchange-correlation potential that permits the total non-Coulombic electron−electron interaction energy, E_{XC}, to be represented as a functional of the electronic charge density, $E_{XC}[\rho]$. Like the Hartree−Fock−Roothaan equations, solution of the Kohn−Sham equations proceeds iteratively via a self-consistent field (SCF) scheme.

Exact functional forms for $E_{XC}[\rho]$ are not known, unfortunately, so approximate forms must be used. Furthermore, once an approximate form is selected there is no prescription for its systematic improvement. It is this fact that points out the principal difference between the Hartree−Fock−Roothaan and Kohn−Sham equations; *while solutions to the former may be viewed as exact solutions to an approximate description, the latter are approximations to an exact description!*

While a number of approximate functionals have been proffered in the literature, the most important can be attributed to Slater[17] and Vosko et al.[18] Slater, using the homogeneous electron gas as a model, developed the following expression for the exchange energy:

$$E_X^S = -\frac{9}{4}\alpha\left[\frac{3\pi}{4}\right]^{1/3}(\rho_\alpha^{4/3} + \rho_\beta^{4/3}) \qquad (3)$$

Here ρ_α and ρ_β are the respective α- and β-electronic charge densities, and α is a parameter (originally assigned the value of $^2/_3$). Using the same model of a homogeneous electron gas, Vosko et al. produced a series of analogous expressions for the correlation energy of the general form

$$E_C^{VWN} = (\rho_\alpha + \rho_\beta)\epsilon(x,\varsigma) \qquad (4a)$$

where

$$x = \left[\frac{3}{4\pi\rho}\right]^{1/6} \qquad \varsigma = \frac{\rho_\alpha - \rho_\beta}{\rho} \qquad (4b)$$

Note that in both of the above energetic expressions, there is only a zeroth-order dependence of the respective energies on the electronic charge density. Functionals possessing such zeroth-order dependence have come to be known as *local* functionals. Taken together, the functionals of Slater (exchange) and Vosko et al. (correlation) are usually referred to as the local (spin) density approximation, L(S)DA:

$$E_{XC}^{L(S)DA} = E_X^S + E_C^{VWN} \qquad (5)$$

Real electronic systems are rarely as homogeneous as those upon which the L(S)DA model is based. To deal with inhomogeneities in the electronic charge density, a number of corrections have been proposed. The most popular approaches toward this problem of an inhomogeneous charge density have involved a gradient correction to the electronic charge density, $\nabla\rho$. Such first-order corrections are commonly referred to as being *nonlocal* in character. While gradient corrections have been implemented for both exchange and correlation functionals, their impact has been most dramatic when applied to the former. The most important of these nonlocal exchange functionals are attributable to Becke[19] and Perdew.[20] The most widely used nonlocal correlation functionals are due to Lee et al.,[21] Perdew,[22] and Perdew and Wang.[23]

Given the foregoing, it is possible to write a general expression for the approximate exchange-correlation energy, $\tilde{E}_{XC}$:

$$\tilde{E}_{XC} = E_X^L[\rho] + E_X^{NL}[\rho,\nabla\rho] + E_C^L[\rho] + E_C^{NL}[\rho,\nabla\rho] \qquad (6)$$

where the superscripts L and NL are used to denote local and nonlocal functionals, respectively.

TABLE 1: Relative Energies (kcal/mol) at 0 K of Relevant Stationary Points on the Potential Energy Surfaces for the Three Pathways ($E2_{anti}$, $E2_{syn}$, and S_N2) Examined in this Study

level of theory[a]	reactants[b]	ion−molecule complex[c]	anti elimination TS	syn elimination TS	S_N2 TS	products[d]
Xα (α = 0.7)	0.0	−24.1	na[e]	−9.6	−9.6	−30.8
S-null	0.0	−23.6	na[e]	−10.3	−9.9	−31.4
B-null	0.0	−12.6	−8.2	0.0	−2.0	−35.6
B-VWN	0.0	−13.8	−7.1	0.3	−2.5	−33.9
B-VWN5	0.0	−13.6	−7.3	0.3	−2.3	−34.2
B-PL	0.0	−13.6	−7.4	0.2	−2.4	−34.2
B-LYP	0.0	−16.4	na[e]	−3.4	−5.4	−33.5
B-P86	0.0	−17.6	na[e]	−3.7	−5.1	−31.6
B-PW91	0.0	−16.4	na[e]	−2.2	−3.5	−31.4
B3-LYP	0.0	−15.9	na[e]	0.7	−1.7	−32.1
B3-P86	0.0	−16.8	na[e]	0.4	−1.6	−30.2
G2+	0.0	−16.5	−3.1	4.2	−0.3	−33.1

[a] DFT energies: DFT/aug-cc-pVDZ + ZPE (unscaled). See text and ref 30 for a description of the G2+ energy. [b] $F^- + CH_3CH_2F$. [c] $F^-\cdot\cdot CH_3CH_2F$. [d] $HF_2^- + CH_2{=}CH_2$. [e] Not available. A TS was not found at this level of theory despite extensive efforts. See text for additional details.

Method. Full geometry optimizations were performed with two different double split-valence basis sets which include polarization functions on both second-row atoms and hydrogen: Pople's 6-31+G(d,p) and Dunning's augmented correlation-consistent aug-cc-pVDZ bases.[24,25] To describe adequately the anionic nature of the current systems, these basis sets also include diffuse functions. In the former case, a single set of diffuse (sp) functions are added to the second-row atoms, and in the latter instance, diffuse functions are added to both second-row atoms (spd) and hydrogen (sp). Vibrational analyses were subsequently carried out with the above bases so as to ascertain the curvature of the potential energy surfaces in the vicinity of the stationary points and to determine zero-point energies. Finite temperature corrections, however, were not applied. Single-point energy calculations were also performed upon all reactant and product species with the 6-311+G(3df,2p) and aug-cc-pVTZ triple split-valence bases.

A variety of local and nonlocal exchange and correlation functionals were employed. As a way of assessing the impact of exchange in the absence of correlation, computations were carried out with the local exchange functionals S-null ($\alpha = {}^2/_3$)[17] and Xα ($\alpha = 0.7$)[17] as well as with B-null,[19] where Becke's gradient correction has been applied to Slater's local exchange functional, S-null. B-null was also used in conjunction with a number of correlation functionals. These include: the local functionals of Vosko, Wilk, and Nusair (VWN and VWN5)[18] and Perdew (PL);[26] and the nonlocal functionals of Lee, Yang, and Paar (LYP),[21] Perdew (P86),[22] and Perdew and Wang (PW91).[23] Two "hybrid" functionals were also used: Becke3-LYP (B3-LYP) and Becke3-P86 (B3-P86).[27] These functionals are termed "hybrids" because they employ both Hartree−Fock and density functional descriptions of the exchange energy. The justification for this combination is the belief that density functional methods fail to account adequately for the self-interaction exchange energy. The relative contributions of exchange (Hartree−Fock, local, and nonlocal) and correlation (local and nonlocal) have been parametrically fit to an empirical data set.

High-level *ab initio* computations were performed in addition to the above density functional calculations. These computations employed a modified G2[28] procedure and are referred to as "G2+". A detailed prescription for the G2+ method can be founded in the literature.[29] Briefly, fully optimized structures are determined at the MP2(fc)/6-31+G(d,p) or MP2(fc)/6-31G(d,p) level for anions and neutrals, respectively. A series of single-point energy calculations, involving larger basis sets and more sophisticated treatments of electron correlation, are subsequently carried out upon these structures. An additivity scheme is then used to generate an effective QCISD(T)/6-311+G(3df,2p) energy. A zero-point energy correction (scaled by 0.9) is also determined at the HF/6-31+G(d,p) level or HF/6-31G(d,p) depending on whether the species is an anion or a neutral. These G2+ calculations will serve as points of reference for the current system in the absence of firm experimental data (e.g., the enthalpies associated with transition states and ion−molecule complexes).[30]

All of the present calculations were carried out with the Gaussian suite of programs (G92/DFT and G94)[31] on HP, IBM, and SGI workstations as well as Cray supercomputers at the Minnesota Supercomputer Institute.

Results

The potential energy surfaces corresponding to the elimination (anti and syn) and substitution pathways for the reaction of fluoride with ethyl fluoride have been studied within the density functional and *ab initio* formalisms. Only the entrance channels (reactants, initial ion−molecule complexes, and transition states (TS's)) and products were investigated in detail as these regions are the most germane in evaluating the relative competitiveness and overall thermicity for the three pathways.

Table 1 lists the zero-point energy corrected relative energies for the reactants, initial ion−molecule complex ($F^-\cdot\cdot CH_3CH_2F$), transition structures, and products. The G2+ energies have also been included for comparison purposes (absolute energies may be found within the Supporting Information). Figure 2 presents generalized structures for the species of interest. The relevant geometrical parameters, principally those directly tied to the reaction coordinates, and point-group symmetries are also defined within the figure. These geometrical parameters are listed in Tables 2−4. The imaginary frequencies corresponding to the transition structures are also included in Tables 3−4 (complete Cartesian coordinate specifications for all structures are given in the Supporting Information).

In an attempt to assess the accuracy of the various levels of theory, the enthalpies for a number of thermochemical processes with known experimental values have been computed.[32] These calculated and experimental values are listed in Tables 5 and 6. Again, the calculated values have been zero-point energy corrected.

Discussion

Before examining the potential energy surfaces predicted by the various density functionals for the reaction of fluoride with ethyl fluoride, a check of the reliability of the functionals to reproduce known thermochemical values is warranted. Given the lack of experimental data on the current system, such a cursory study is made all the more imperative. Four related reactions which have known enthalpies were used as bench-

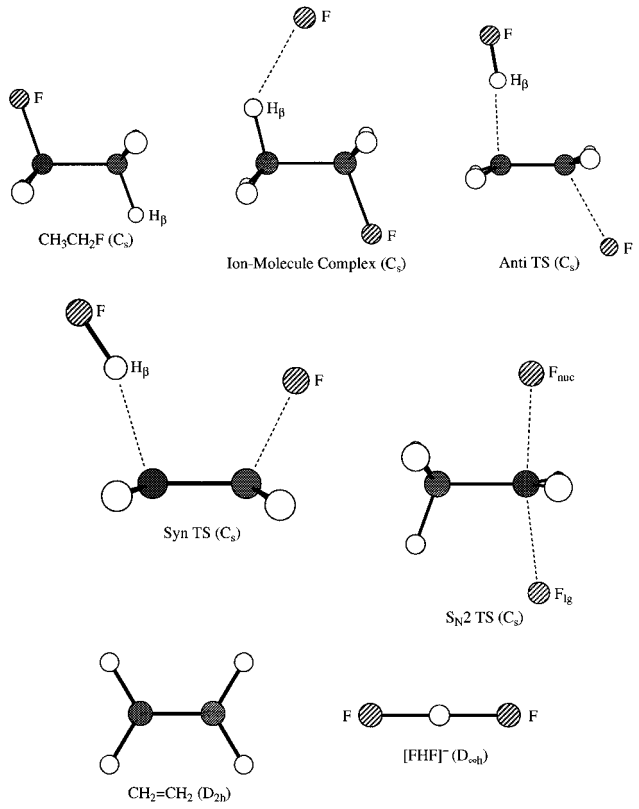

Figure 2. Reactant, transition-state, and product structures.

marks for the energetics of interest in the current study.[33]

$$HF \rightarrow F^- + H^+ \quad (7)$$

$$CH_3CH_2F \rightarrow HF + CH_2{=}CH_2 \quad (8)$$

$$F^- + CH_3CH_2F \rightarrow [FHF]^- + CH_2{=}CH_2 \quad (9)$$

$$[FHF]^- \rightarrow HF + F^- \quad (10)$$

Again, structural optimizations and vibrational analyses were performed with double split-valence basis sets (i.e., 6-31+G(d,p) and aug-cc-pVDZ); single-point calculations were subsequently performed with triple split-valence basis sets (i.e., 6-311+G(3df,2p) and aug-cc-pVTZ).

The calculated proton affinities (PA) for fluoride (eq 7) with the double split-valence bases are all too exothermic (Tables 5 and 6), often by an appreciable amount (e.g., the functionals without a correlation component). An increase in basis set quality, from a double to triple split, reduces the magnitude of this error by an average of 3.4 and 2.2 kcal/mol for the Pople and Dunning bases, respectively. The smallest errors are obtained with the hybrid functional B3-P86 regardless of which basis set is used. Local correlation functionals (B-VWN, B-VWN5, and B-PL) and one of the nonlocally correlated functionals (B-PW91) also perform fairly well, especially with the triple split bases. Smaller errors are consistently obtained with the Pople bases while there appears to be a greater degree of convergence with the Dunning bases. Moreover, these five functionals give similar results to the high-level *ab initio* calculation (G2+), and both methods provide values within the G2 target accuracy of ±2 kcal/mol. None of the proton affinities, however, are within the experimental range of uncertainty.

The computed enthalpies for the elimination of hydrogen fluoride from ethyl fluoride (eq 8) with the double split-valence bases are somewhat more accurate (on average by 2.7 and 4.1 kcal/mol for the Pople and Dunning bases, respectively) than the proton affinities for fluoride. The biggest improvement is for the S-null and B-LYP functionals. All of the DFT methods, however, show increased convergence. As a result, there is only a 1.9 kcal/mol improvement with the Dunning triple split-valence basis set and the error actually gets worse by 0.9 kcal/mol with the 6-311+G(3df,2p) basis set. Moreover, the enthalpies are no longer systematically too exothermic; B-null, B-LYP, and the locally correlated functionals give enthalpies which are too small while the other functionals yield values which are too large (i.e., endothermic). The best results are obtained with the functionals incorporating nonlocal correlation (B-LYP, B-P86, and B-PW91) and the hybrid functional, B3-LYP. The performance of the locally correlated functionals is somewhat less reliable. Once again, the error associated with the G2+ calculation is comparable to the best DFT results and the agreement with experiment falls within the G2 target accuracy, if not within the experimental uncertainty.

The most exothermic pathway for the current system of interest ($F^- + CH_3CH_2F$) is represented by eq 9. All of the

TABLE 2: Geometrical Parameters for CH_3CH_2F, $CH_2{=}CH_2$, and $[FHF]^-$ in Figure 2[a]

A. CH_3CH_2F (C_s)

level of theory[b]	r_{CH_β}	r_{CC}	r_{CF}	$\angle CCH_\beta$	$\angle CCF$	θ_α[c]	θ_β[c]
Xα (α = 0.7)	1.113	1.500	1.396	109.9	109.8	50.0	52.3
S-null	1.127	1.519	1.415	109.8	109.8	50.0	52.3
B-null	1.121	1.551	1.464	109.1	109.8	48.5	52.1
B-VWN	1.102	1.526	1.439	109.2	109.9	48.8	52.1
B-VWN5	1.103	1.528	1.441	109.2	109.9	48.8	52.1
B-PL	1.104	1.529	1.441	109.3	109.9	49.0	52.1
B-LYP	1.107	1.524	1.436	109.4	109.7	48.7	52.3
B-P86	1.108	1.518	1.424	109.4	109.8	49.3	52.1
B-PW91	1.106	1.517	1.422	109.4	110.0	49.6	52.1
B3-LYP	1.100	1.514	1.413	109.5	109.7	49.4	52.4
B3-P86	1.099	1.507	1.402	109.6	109.9	49.8	52.4
G2+	1.089	1.509	1.398	110.3	109.4	51.1	53.6

B. $CH_2{=}CH_2$ (D_{2h})

level of theory[b]	r_{CC}	r_{CH}	$\angle CCH$
Xα (α = 0.7)	1.337	1.105	121.6
S-null	1.351	1.119	121.6
B-null	1.362	1.110	121.8
B-VWN	1.342	1.092	121.8
B-VWN5	1.344	1.094	121.8
B-PL	1.345	1.095	121.8
B-LYP	1.345	1.098	121.8
B-P86	1.344	1.100	121.7
B-PW91	1.342	1.098	121.7
B3-LYP	1.335	1.091	121.7
B3-P86	1.333	1.091	121.6
G2+	1.335	1.081	121.6

C. $[FHF]^-$ ($D_{\infty h}$)

level of theory[b]	r_{HF}
Xα (α = 0.7)	1.156
S-null	1.172
B-null	1.193
B-VWN	1.171
B-VWN5	1.174
B-PL	1.174
B-LYP	1.171
B-P86	1.167
B-PW91	1.166
B3-LYP	1.155
B3-P86	1.150
G2+	1.150

[a] All bond lengths in angstroms and angles in degrees. [b] DFT/aug-cc-pVDZ geometries except for the MP2(fc)/6-31+G(d,p) (G2+) structure. [c] Acute angle formed by the bisector of ∠HCH and r_{CC}.

TABLE 3: Geometrical Parameters for the Ion−Molecule Complex and Elimination Transition-State Structures (syn and anti) in Figure 2[a]

A. Ion−Molecule Complex (C_s)

level of theory[b]	r_{CH_β}	r_{CC}	r_{CF}	r_{FH_β}	$\angle CCH_\beta$	$\angle CCF$	$\angle FH_\beta C$[c]	θ_α[d]	θ_β[d]
Xα (α = 0.7)	1.216	1.474	1.449	1.439	105.9	114.5	175.1	50.4	50.0
S-null	1.233	1.491	1.472	1.455	106.0	114.5	175.3	50.1	50.1
B-null	1.149	1.532	1.516	1.851	106.5	112.7	170.9	48.0	51.8
B-VWN	1.136	1.506	1.486	1.763	106.2	112.9	170.2	48.6	51.6
B-VWN5	1.138	1.508	1.490	1.764	106.5	112.9	172.2	48.4	51.6
B-PL	1.138	1.510	1.490	1.776	106.3	112.9	170.1	48.5	51.6
B-LYP	1.157	1.502	1.487	1.659	106.1	113.2	171.6	48.6	51.4
B-P86	1.173	1.495	1.475	1.589	106.5	113.8	174.8	49.2	51.2
B-PW91	1.168	1.495	1.473	1.605	106.8	113.6	175.1	49.3	51.4
B3-LYP	1.136	1.498	1.451	1.704	105.6	112.8	166.7	50.0	52.1
B3-P86	1.147	1.490	1.441	1.632	106.0	113.3	170.7	50.3	51.8
G2+	1.096	1.499	1.452	2.004	103.9	110.5	136.5	49.6	53.0

B. Anti Elimination TS (C_s)

level of theory[b]	r_{CH_β}	r_{CC}	r_{CF}	r_{FH_β}	$\angle CCH_\beta$	$\angle CCF$	$\angle FH_\beta C$[c]	θ_α[d]	θ_β[d]	*i* freq
B-null	1.603	1.443	1.829	1.104	104.8	116.6	185.1	32.8	37.3	242
B-VWN	1.767	1.387	2.045	1.010	97.2	117.9	187.1	19.8	23.0	54
B-VWN5	1.721	1.397	1.968	1.027	99.6	117.3	186.4	24.0	27.0	74
B-PL	1.725	1.398	1.973	1.026	99.5	117.4	186.5	23.8	26.8	72
G2+	1.811	1.373	1.990	0.981	91.8	118.3	188.3	21.3	21.8	332

C. Syn Elimination TS (C_s)

level of theory[b]	r_{CH_β}	r_{CC}	r_{CF}	r_{FH_β}	$\angle CCH_\beta$	$\angle CCF$	$\angle FH_\beta C$[c]	θ_α[d]	θ_β[d]	*i* freq
Xα (α = 0.7)	1.904	1.387	1.781	0.989	90.5	114.5	211.5	26.8	0.0	417
S-null	1.927	1.402	1.808	1.001	92.0	114.5	210.4	26.4	0.0	371
B-null	1.602	1.468	1.703	1.101	118.7	114.6	190.7	34.3	40.5	386
B-VWN	1.625	1.429	1.736	1.054	116.9	115.5	191.4	31.7	33.7	322
B-VWN5	1.623	1.433	1.730	1.059	117.2	115.4	191.3	32.1	34.6	326
B-PL	1.623	1.434	1.732	1.059	117.2	115.4	191.3	32.1	34.6	325
B-LYP	1.691	1.417	1.773	1.031	114.1	115.9	193.3	29.5	25.1	248
B-P86	1.866	1.386	1.955	0.986	104.3	118.0	202.4	20.0	6.0	126
B-PW91	1.833	1.389	1.925	0.989	107.2	117.9	199.7	21.8	8.6	131
B3-LYP	1.781	1.401	1.758	0.991	110.0	116.2	195.1	29.5	17.0	267
B3-P86	1.857	1.381	1.848	0.971	103.9	117.2	201.2	24.4	6.0	219
G2+	1.808	1.402	1.704	0.984	107.8	115.9	196.0	32.4	19.3	393

[a] All bond lengths in angstroms, angles in degrees, and frequencies in cm^{-1}. [b] DFT/aug-cc-pVDZ geometries except for the MP2(fc)/6-31+G(d,p) (G2+) structure. [c] $\angle FH_\beta C \leq 180°$, $\angle FH_\beta CC = 0°$; $\angle FH_\beta C > 180°$, $\angle FH_\beta CC = 180°$. [d] Acute angle formed by the bisector of $\angle HCH$ and r_{CC}.

TABLE 4: Geometrical Parameters for the S_N2 Transition-State Structure (C_s) in Figure 2[a]

level of theory[b]	$r_{CF_{nuc}}$	$r_{CF_{lg}}$	$\angle CCF_{nuc}$	$\angle CCF_{lg}$	*i* freq
Xα (α = 0.7)	1.835	1.835	94.5	94.6	422
S-null	1.863	1.864	94.7	94.7	403
B-null	1.986	2.026	98.2	94.8	339
B-VWN	1.934	1.971	97.7	94.3	359
B-VWN5	1.940	1.977	97.8	94.5	357
B-PL	1.941	1.978	97.8	94.4	356
B-LYP	1.909	1.943	97.3	93.8	364
B-P86	1.879	1.909	96.9	93.4	384
B-PW91[c]	1.898	1.898	95.4	95.4	388
B3-LYP	1.876	1.898	96.9	93.5	455
B3-P86	1.850	1.868	96.6	93.2	473
G2+	1.855	1.865	96.7	92.8	615

[a] All bond lengths in angstroms, angles in degrees, and frequencies in cm^{-1}. [b] DFT/aug-cc-pVDZ geometries except for the MP2(fc)/6-31+G(d,p) (G2+) structure. [c] C_1 structure.

functionals, with one notable exception (B3-P86), succeed in reproducing the experimental enthalpy, more often than not yielding values within the experimental uncertainty. Given the high degree of basis set convergence, this agreement is fairly independent of the basis set chosen. It is interesting to note that functionals that had performed poorly to this point do an acceptable job in reproducing the energetics associated with this pathway. Such agreement is most probably attributable to a fortuitous cancellation of errors. The best results are obtained with the locally correlated functionals as was found for the

TABLE 5: Density Functional with Dunning's Basis Sets, G2+, and Experimental Enthalpies of Reaction for Related Thermochemical Processes[a]

level of theory	ΔH_{rxn} (eq 7)	ΔH_{rxn} (eq 8)	ΔH_{rxn} (eq 9)	ΔH_{rxn} (eq 10)
Xα (α = 0.7)	357.4 (359.4)	20.5 (19.6)	−30.8 (−31.7)	51.3 (51.3)
S-null	352.9 (354.8)	18.2 (17.4)	−31.4 (−32.1)	49.7 (49.5)
B-null	359.1 (361.1)	1.7 (0.7)	−35.6 (−36.5)	37.3 (37.2)
B-VWN	366.5 (368.7)	6.8 (5.8)	−33.9 (−35.1)	40.7 (40.9)
B-VWN5	365.6 (367.8)	6.1 (5.1)	−34.2 (−35.3)	40.2 (40.4)
B-PL	365.5 (367.7)	6.1 (5.1)	−34.2 (−35.3)	40.2 (40.4)
B-LYP	360.9 (363.1)	10.1 (9.1)	−33.5 (−34.5)	43.6 (43.6)
B-P86	364.2 (366.3)	13.2 (12.5)	−31.6 (−32.4)	44.8 (44.9)
B-PW91	365.7 (368.0)	12.3 (11.5)	−31.4 (−32.3)	43.7 (43.7)
B3-LYP	364.7 (367.1)	12.3 (11.6)	−32.1 (−33.0)	44.4 (44.7)
B3-P86	368.1 (370.4)	15.5 (15.0)	−30.2 (−31.1)	45.7 (46.1)
G2+	372.2	12.2	−33.1	45.2
experiment[b]	371.5 ± 0.2	10.2 ± 0.9	−35.6 ± 3.1	45.8 ± 1.6

[a] All values in kcal/mol. DFT energies: DFT/aug-cc-pVDZ + ZPE (unscaled); parenthetical values DFT/aug-cc-pVTZ//DFT/aug-cc-pVDZ + ZPE (unscaled). See the text and ref 30 for a description of the G2+ energy and the various reactions. All of the calculated values are at 0 K. [b] Experimental values are from ref 32 except for ΔH_{rxn} (eq 10), which comes from ref 34.

proton affinity of fluoride. The G2+ value is also in excellent accord with experiment.

The final reaction examined (eq 10) corresponds to the fluoride affinity of hydrogen fluoride. This quantity has recently been the subject of both experimental and theoretical investiga-

TABLE 6: Density Functional with Pople's Basis Sets, G2+, and Experimental Enthalpies of Reaction for Related Thermochemical Processes[a]

level of theory	ΔH_{rxn} (eq 7)	ΔH_{rxn} (eq 8)	ΔH_{rxn} (eq 9)	ΔH_{rxn} (eq 10)
Xα (α = 0.7)	358.5 (362.0)	21.8 (20.0)	−32.1 (−33.2)	53.9 (53.2)
S-null	354.3 (357.9)	19.5 (17.7)	−32.9 (−33.9)	52.4 (51.6)
B-null	361.0 (364.4)	2.8 (1.1)	−37.4 (−37.9)	40.1 (39.0)
B-VWN	367.5 (370.9)	7.9 (5.9)	−35.3 (−36.2)	43.2 (42.1)
B-VWN5	366.8 (370.2)	7.2 (5.3)	−35.6 (−36.4)	42.8 (41.7)
B-PL	366.6 (370.0)	7.2 (5.2)	−35.6 (−36.4)	42.8 (41.7)
B-LYP	362.2 (365.7)	11.3 (9.3)	−34.9 (−35.9)	46.2 (45.2)
B-P86	365.1 (368.4)	14.3 (12.7)	−32.9 (−33.6)	47.2 (46.3)
B-PW91	366.8 (370.1)	13.2 (11.8)	−32.9 (−33.3)	46.1 (45.1)
B3-LYP	365.5 (368.9)	13.5 (11.9)	−33.2 (−33.8)	46.7 (45.7)
B3-P86	368.5 (371.8)	16.5 (19.2)	−31.3 (−27.7)	47.9 (46.9)
G2+	372.2	12.2	−33.1	45.2
experiment[b]	371.5 ± 0.2	10.2 ± 0.9	−35.6 ± 3.1	45.8 ± 1.6

[a] All values in kcal/mol. DFT energies: DFT/6-31+G(d,p) + ZPE (scaled by 0.9); parenthetical values DFT/6-311+G(3df,2p)//DFT/6-31+G(d,p) + ZPE (scaled by 0.9). See the text and ref 30 for a description of the G2+ energy and the various reactions. All of the calculated values are at 0 K. [b] Experimental values are from ref 32 except for ΔH_{rxn} (eq 10) which comes from ref 34.

tions, and now seems to be fairly well established.[34] The best agreement with experiment is found for the hybrid and nonlocally correlated functionals. While there is still a sizable error associated with the local exchange functionals (Xα and S-null), a significant reduction in this error is readily apparent; this is again presumably due to some cancellation of errors. As has been observed above for eqs 8 and 9, only a slight improvement is seen when the larger triple split-valence bases are used (and only for some of the functionals). The G2+ calculation gives a value within the experimental error.

From the foregoing discussion, a number of salient observations can be noted: (1) No single functional, let alone a class of functionals, consistently reproduces the above experimental values. Moreover, the errors associated with the functionals appear to be random in nature and, thus, offer no immediately apparent clue that would suggest how to improve them systematically. It is also equally clear that functionals lacking Becke's gradient correction to the exchange term and which fail to take into account correlation perform in an inferior fashion. (2) The high-level *ab initio* calculation (G2+) yields values that are consistently within a few kcal/mol of those experimentally determined. Given this apparent high degree of accuracy, coupled with the dearth of experimental data on the $F^- + CH_3CH_2F$ potential energy surface, it seems reasonable to use the results from the G2+ calculations as a standard by which to gauge the performance of various levels of density functional theory. (3) In terms of a "cost-benefit" analysis, the calculation of single-point energies with triple split-valence bases on top of the double split-valence optimizations does not seem to be called for; the overall error is reduced by only 0.7 kcal/mol. This conclusion is quantitatively supported in Table 7, which provides a statistical analysis of the basis set dependence. It also is consistent with numerous observations in the literature that density functional methods tend to converge to the infinite basis set limit more rapidly than traditional *ab initio* methods.[35] As such, the following discussion is for the DFT potential energy surfaces obtained with Dunning's aug-cc-pVDZ basis set. We will note, however, where a larger basis set may be expected to have an impact and where the use of the 6-31+G(d,p) basis set leads to different results.

A list of energies corresponding to a number of relevant points from the density functional and G2+ potential energy surfaces can be found in Table 1. All of the energies are relative to the separated reactants: $F^- + CH_3CH_2F$. All of the surfaces exhibit the double-well behavior (a barrier separating two minima that correspond to reactant and product ion−molecule complexes) that is characteristic of many gas-phase reactions (see Figure 3). As was noted above, only the entrance channel was examined in detail as the exit channel is likely to be very sensitive to dynamical effects.

TABLE 7: Comparison of Computed and Experimental Energies as a Function of Basis Set Size[a]

	Δerror				
basis set	eq 7	eq 8	eq 9	eq 10	total[b]
Pople	av = 3.4	−0.2	−0.2	−0.1	0.7
	std dev = 0.2	1.9	1.3	0.9	1.9
Dunning	av = 2.2	−0.1	0.8	0.1	0.7
	std dev = 0.2	0.9	0.6	0.2	1.0

[a] Δerror = |error($D\zeta$)| − |error($T\zeta$)|, where $D\zeta$: 6-31+G(d,p) or aug-cc-pVDZ; and $T\zeta$: 6-311+G(3df,2p) or aug-cc-pVTZ. When Δerror has a positive value, there is a decrease in the error with an increase in the basis set size while a negative value indicates an increase in the error upon going to the bigger basis set size (see text for descriptions of eqs 7−10). [b] Statistics for all four reactions.

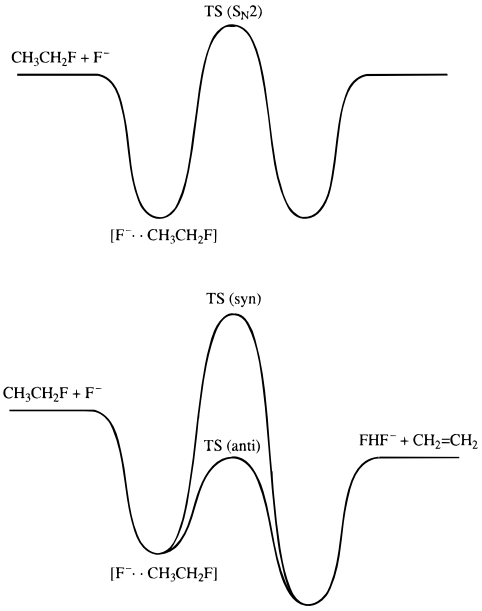

Figure 3. Schematic representations of S_N2 (upper diagram) and anti/syn E2 (lower diagram) reaction coordinates.

Upon reaction of fluoride with ethyl fluoride, an exothermic ion−molecule complex is predicted to form. Clusters of this sort typically have enthalpies of formation between −10 and −20 kcal/mol.[36] For the present system, three important ion−molecule complexes can be envisioned; one corresponding to each of the three reaction pathways (anti and syn elimination and nucleophilic substitution). While each of these three structures was located, only the one corresponding to the anti elimination pathway will be discussed as it is consistently lower in energy than the other two. A range of exothermicities was found for the density functional methods (Table 1). Within a given class of functionals, however, the enthalpies of formation showed little variation. The local exchange functionals (Xα and S-null) again demonstrate their tendency toward overbinding by giving enthalpies that are appreciably too exothermic. This overestimation of the complex stability results from an extremely strong hydrogen bond. At the other end of the spectrum is the value predicted by the B-null functional. Unlike the other two noncorrelated functionals, B-null affords a complexation energy (12.6 kcal/mol) which is consistent with typical experimental

values. The locally correlated functionals yield an average enthalpy of −13.7 kcal/mol, while the nonlocally correlated and hybrid methods lead to somewhat more strongly bound complexes (the average enthalpy is −16.6 kcal/mol). The G2+ calculation gives a similar value, of −16.5 kcal/mol, to the latter DFT procedures. While all the correlated methods predict ion−molecule complexes that are of reasonable stability, the locally correlated functionals yield enthalpies that are most similar to the high-level *ab initio* calculation.

A structural examination of the ion−molecule complexes reveals a substantive difference between the geometries predicted by density functional and *ab initio* methods. The MP2/6-31+G(d,p) structure, which is the basis of the G2+ calculation, is characterized by a lengthy F−H_β bond of over 2 Å with less than a 0.01 Å elongation of the H_β−C bond. The largest geometrical change relative to ethyl fluoride is a 0.05 Å lengthening of the C−F bond. This complex also has a F−H_β−C bond angle of 136.5°, which suggests a quasi-E2C-like interaction, but at this point on the potential energy surface the reaction has not taken place to any significant extent. In contrast, the density functional structures are characterized by shorter F−H_β bond distances (from 0.15 to 0.57 Å relative to that found at the MP2 level), elongated H_β−C bonds (0.04−0.14 Å relative to CH_3CH_2F), and more nearly linear (166.7−175.3°) hydrogen bonds. Like the MP2 structure, those predicted by the density functional methods evince longer C−F bonds. All taken together, the density functional calculations predict a spectrum of $E1_{cb}$-like structures in which the reaction has progressed further along the reaction coordinate. It is also interesting to note that the complexation enthalpies track with the values for r_{CH_β} and r_{FH_β} (i.e., the relative energy of the ion−molecule complex is inversely proportional to r_{CH_β} and directly proportional to r_{FH_β}).

These structural differences become even more pronounced when the transition structures are examined. The most striking of these comparisons involves the anti elimination TS. Transition structures were only found for four of the functionals: B-null, B-VWN, B-VWN5, and B-PL. Moreover, these structures were only located with the aug-cc-pVDZ basis set and not Pople's 6-31+G(d,p) basis set. This represents an extreme case of basis set dependence given that the two bases are similar in size and quality. These results are consistent with those of Bickelhaupt et al., in that they were only able to offer an estimate of the anti elimination transition structure and its energy.[12] Examination of the imaginary frequencies corresponding to the reaction coordinate may offer some insight into this inability to locate anti elimination transition structures. A scaled imaginary frequency of 332 cm^{-1} was determined at the MP2/6-31+G(d,p) level. This frequency softens appreciably when calculated with the density functional methods, which appear to have extreme difficulty in treating low-frequency modes. Given that one of the real successes of DFT has been the accurate prediction of vibrational frequencies,[37] this severe underestimation of these imaginary frequencies (on average by 80% with the locally correlated functionals) may be specific to the unique demands of transition-state searches (*vide infra*).

As one progresses through the density functional transition structures to those predicted at the MP2 level, a gradient of early to late TS's is seen. These changes are apparent by looking at the same geometric parameters discussed above for the ion−molecule complex. In the transition structures a larger decrease in the F−H_β bond is seen, and it is most pronounced in the MP2 structure. Likewise, there is a lengthening of the H_β−C and C−F bonds and a decrease in the C−C bond. A distinct flattening of the carbon skeleton also takes place as these centers formally rehybridize from sp^3 to sp^2. This is indicated by decreased values for θ_α and θ_β (θ is defined as the acute angle formed by the C−C bond and the bisector of either the α or β HCH angle). All told, the various methods predict E2-like TS's that vary from one to another in the extent to which the elimination has taken place: MP2 > B-VWN, B-VWN5, B-PL > B-null.

The G2+ calculation predicts a barrier of 3.1 kcal/mol below the energy of the separated reactants (i.e., $E_a = -3.1$ kcal/mol). The density functional methods yield barriers which are about 4−5 kcal/mol smaller (i.e., $E_a = -7$ to −8 kcal/mol). These energetic results are consistent with the noted structural changes. That is, density functional methods predict earlier transition structures than the high-level *ab initio* calculation.

This underestimation of barrier heights and imaginary frequencies carries over to the syn elimination pathway. The G2+ calculation predicts that the syn elimination should, unlike its anti elimination counterpart, possess a positive activation energy (E_a) of 4.2 kcal/mol. This E_a is most severely underestimated by the uncorrelated functionals and those possessing nonlocal correlation, on average by 14.1 and 7.3 kcal/mol, respectively. Both the locally correlated and hybrid functionals predict essentially barrierless processes, which again underestimate the G2+ value by approximately 4 kcal/mol.

The MP2 vibrational analysis gives an imaginary frequency of 393*i* cm^{-1}, which represents a slightly tighter TS than that found for the anti elimination pathway. The incorporation of correlation (especially of a nonlocal nature) by the density functional methods softens this frequency, although not to the same degree as is seen in the anti elimination TS's. Excluding the noncorrelated functionals, which do surprisingly well at reproducing the MP2 value, the density functionals underestimate this transition frequency by an average of 148*i* cm^{-1} (or by 62%).

The G2+ syn elimination TS has a typical $E1_{cb}$-like structure in which abstraction of the β proton, H_β, has proceeded to a greater extent than the loss of F^-; an appreciable reduction in the F−H_β bond is also evident. In this transition structure, the β-carbon has flattened, the α-carbon is far more pyramidal, and the C−C bond shows a smaller reduction in length than is found in the anti elimination TS.

While the density functional transition structures also display $E1_{cb}$-like character, they are nonetheless shifted toward a more central E2 TS. This is readily apparent by the greater degree of parity in the values for r_{CH_β} and r_{CF}. Once again, a spectrum of TS's is evident for the density functional series: the local exchange and hybrid functionals are the most $E1_{cb}$-like, while the other functionals are more E2-like in nature.

Nucleophilic substitution at the C_α site is predicted by the G2+ calculation to have an E_a of −0.3 kcal/mol. All of the density functional methods predict TS's with more negative activation barriers. In particular, local exchange, nonlocally correlated, locally correlated, and hybrid functionals underestimate, on average, the G2+ value by 9.4, 4.4, 2.1, and 1.4 kcal/mol, respectively. Similarly, the imaginary frequencies corresponding to the S_N2 reaction coordinate are underestimated, this time on average by 224*i* cm^{-1} (or 36%).

The structural differences between the MP2 and density functional level S_N2 transition structures are minor in nature. Most of the functionals predict slightly longer C−F bond lengths and a somewhat greater differential between the two C−F bonds with $r_{CF_{nuc}} > r_{CF_{lg}}$. It is also interesting to note that, while the Xα and S-null functionals do not reproduce the G2+ value for the reaction barrier or the corresponding transition frequency,

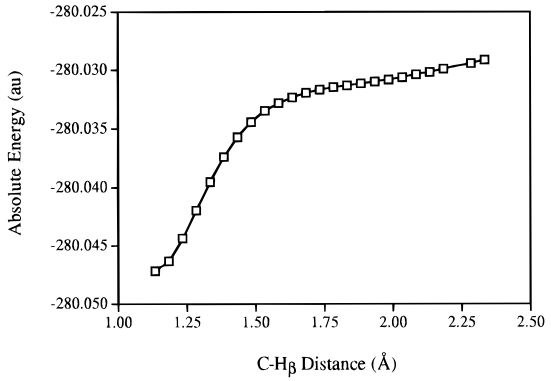

Figure 4. Plot of C−H$_\beta$ distance (Å) vs absolute energy (au) for B-VWN5/6-31+G(d,p) partial optimizations so as to map out the anti elimination TS structure. Optimizations were performed within the C_s point group (see text for details).

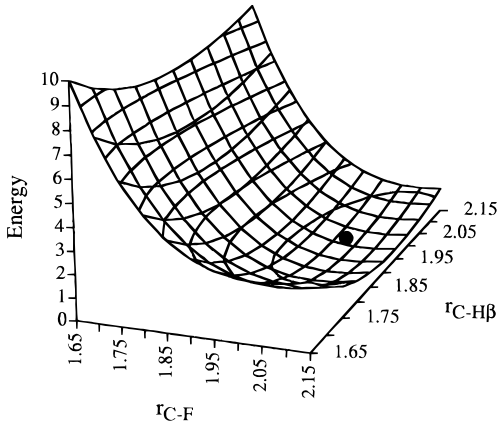

Figure 5. Three-dimensional plot of the relative energy as a function of C−H$_\beta$ and C−F from B-VWN5/6-31+G(d,p) partial optimizations. All energies and distances are in kcal/mol and angstroms, respectively. The "minimum" is indicated by the black circle (see text for details).

they do, nevertheless, show a great deal of fidelity with the MP2 structure.

Anti Elimination TS Search. Numerous attempts were made to locate density functional transition-state (TS) structures for the anti elimination pathway. With the exception of efforts involving the aug-cc-pVDZ basis set *and* the four functionals B-null, B-VWN, B-VWN5, and B-PL, no such TS structures were ever located. This extreme basis set and functional dependence is perhaps the most salient result to come from this study, and as such a brief discussion outlining the methods used in the search for this elusive TS structure is warranted. Unless noted otherwise in the discussion that follows, the B-VWN5/6-31+G(d,p) level of theory was employed. While other functionals were examined, none were studied in as great detail as B-VWN5 and Xα. The former functional was chosen for the ensuing TS searches primarily because of the relative ease with which its wave functions were converged. This decision was shown to be prudent as the sought after TS structure was eventually located with this family of functionals (B-null, B-VWN, B-VWN5, and B-PL) and the aug-cc-pVDZ basis set. The TS structure searches with the B-VWN5 functional were also repeated with the Xα functional so that the results of Bickelhaupt et al.[12] could be more directly compared. The results obtained with the Xα functional closely parallel those found with the B-VWN5 functional and, therefore, will not be discussed at present.

After several attempts at full optimizations with a variety of local and nonlocal density functionals failed to yield the desired TS structure, a series of partial optimizations were undertaken in which the C−H$_\beta$ distance was fixed while the remainder of the structure was allowed to relax. The C−H$_\beta$ distance was stepped in 0.05 Å increments over a range from 1.135 (the optimized distance in the ion−molecule complex) to 2.335 Å. The system was initially constrained within the C_s point group. As can be clearly seen in Figure 4, there is no indication of any new stationary local minima or maxima. The symmetry constraint was subsequently relaxed, and a series of C_1 symmetry partial optimizations were repeated over an extended C−H$_\beta$ range of 1.135−2.880 Å. Once again, a curve similar to that found in Figure 4 was generated which revealed no new stationary local minima or maxima (it should be added that as the C−H$_\beta$ distance was increased, it became more and more difficult to achieve wave function convergence, a common problem with density functional calculations).

Upon closer examination of the plot in Figure 4, it is possible to glean some very *qualified* information with respect to the TS structure. The plot reveals two nearly linear regions of differing slope: the first between (C−H$_\beta$) 1.185 and 1.485 Å; the second between 1.685 and 2.135 Å. Linear regression analysis produced the following two equations:

$$y = 0.041x - 280.095 \qquad (\text{C}-\text{H}_\beta = 1.185-1.485\ \text{Å})$$

$$y = 0.004x - 280.038 \qquad (\text{C}-\text{H}_\beta = 1.685-2.135\ \text{Å})$$

where y is the absolute energy in hartrees, and x is the C−H$_\beta$ distance in angstroms. Simultaneous solution of the two equations yields a C−H$_\beta$ distance of 1.541 Å and an absolute energy of −280.03184 au. This energy translates into a barrier that is 4.4 kcal/mol lower in energy than the separated reactants (not ZPE corrected), which is similar to the DFT/aug-cc-pVDZ barriers of −4 to −5 kcal/mol (not ZPE corrected).

A potential energy surface was also mapped out as a function of the (chemically intuitive) most important two distances: C−H$_\beta$ and C−F. Each coordinate of the surface spanned a range from 1.65 to 2.15 Å. Partial optimizations (121 of them) were carried out in which the two distances were fixed in 0.05 Å increments while the rest of the structure was allowed to relax fully. Examination of the surface (Figure 5) revealed a contour that sloped downward as the C−F distance increased. A very shallow local "minimum" (i.e., a possible saddle point) was found in the vicinity of (C−H$_\beta$ = 1.925 Å, C−F = 2.075 Å). A series of full optimizations were performed in this area to locate the TS, but even with the accurate determination of force constants, the system rapidly dissociated to the products or collapsed to the reactant ion−molecule complex. The desired TS structure was never successfully located, and the "minimum" in Figure 5 appears to be an artifact of how the surface was obtained (i.e., partial optimizations).

Becke has argued for the necessity of including Hartree−Fock exchange in the construction of density functionals.[27,38] This has led to his development of the so-called "hybrid" functionals (*vide supra*). To assess the role that Hartree−Fock exchange may play in the location of the anti elimination TS structure, a series of *full* optimizations were carried out in which the amount of Hartree−Fock exchange was varied. The results from these calculations are presented in Table 8. *Over a range of Hartree−Fock to Becke88 (i.e., B-null) exchange ratios of 999:1 to 1:9, it was possible to locate the elusive TS structure!* At ratios with values lower than 1:9, TS structures could not be found, and the optimizations either led back to the reactant ion−dipole complex or to the reaction products. Table 8 also lists the energy of the TS relative to the separated reactants as a function of the ratio of exchange (it is important to note that in order to facilitate a proper comparison between reactant and

TABLE 8: B-VWN5 plus Hartree−Fock Exchange Data for the anti Elimination Transition Structure[a]

HF:B88	E (opt)[b]	E (sp)[c]	ΔE[d]	eigenvalue[e] (force constant)	F−H$_\beta$	H$_\beta$−C	C−C	C−F
1:9	−280.01135	−280.03121	−4.0	−0.00110	0.998	1.800	1.382	2.064
1:3	−279.98401	−280.03051	−3.6	−0.00663	0.993	1.779	1.383	1.950
1:1	−279.94521	−280.02830	−2.2	−0.01862	0.973	1.800	1.376	1.891
3:1	−279.91395	−280.02551	−0.5	−0.04701	0.955	1.821	1.368	1.861
9:1	−279.89840	−280.02368	0.7	−0.05487	0.947	1.831	1.364	1.849
19:1	−279.89371	−280.02304	1.1	−0.05771	0.944	1.833	1.362	1.845
99:1	−279.89013	−280.02253	1.4	−0.05809	0.942	1.835	1.361	1.842
999:1	−279.88934	−280.02253	1.4	−0.06106	0.942	1.835	1.361	1.842

[a] Ratio of Hartree−Fock (HF) to Becke88 (B88) exchange ranges from 999:1 to 1:9. For ratios smaller than 1:9, TS structures were not found. Absolute energies in hartrees, relative energies in kcal/mol, and distances in angstroms. [b] Energies associated with full optimizations using the B-VWN5 functional and Hartree−Fock exchange. [c] Single-point energies using the B-VWN5 functional without Hartree−Fock exchange are based upon fully optimized (B-VWN5 + HF) structures. [d] Relative energy difference between the anti elimination TS and the separated reactants (not ZPE corrected). [e] Eigenvalues are in au.

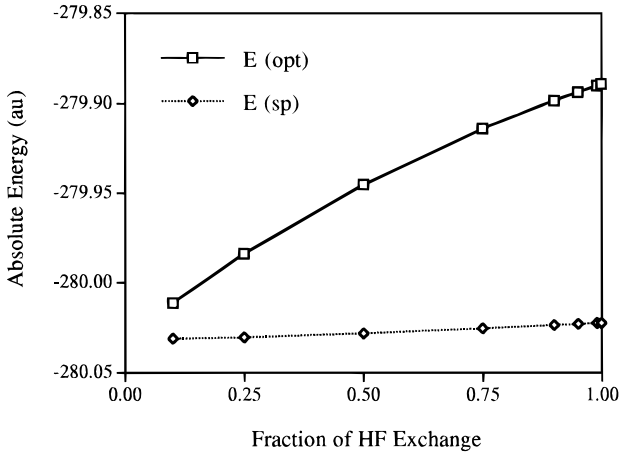

Figure 6. Plot of the fraction of Hartree−Fock exchange energy used in B-VWN5/6-31+G(d,p) full optimizations of the anti elimination transition-state structure. The upper curve corresponds to the absolute energy obtained from the optimization while the lower curve represents the absolute energy obtained from a single-point calculation. Linear equations (y is absolute energy and x is the fraction of Hartree−Fock exchange): optimization curve, $y = 0.133x - 280.018$, $r^2 = 0.991$; single-point curve, $y = 0.010x - 280.033$, $r^2 = 0.990$ (see text for details).

TS structures, single-point calculations that made no use of Hartree−Fock exchange were performed on the optimized TS structures). As the percentage of Becke88 exchange was increased, the barrier to elimination decreased from +1.4 kcal/mol (999:1) to −4.0 kcal/mol (1:9). What is particularly fascinating is that the G2+ calculation predicts a barrier that is −0.7 kcal/mol (not ZPE corrected) above the separated reactants. This corresponds to a ratio of Hartree−Fock to Becke88 of between 1:1 to 3:1. Becke has recently offered a value of about 1:3;[38] this prescription would yield an extrapolated value for the barrier height around −3.1 kcal/mol (see Figure 6).

Still more interesting is the effect density functional exchange has upon the Hessian eigenvalue associated with TS reaction coordinate. As the ratio of Hartree−Fock to Becke88 exchange decreases, the value of this eigenvalue becomes more positive. This translates into a flatter reaction coordinate (and a smaller TS imaginary frequency) and may, thus, help to explain the difficulty that density functional theory has in locating the anti elimination TS structure (note that at the B-VWN5/aug-cc-pVDZ level of theory the value for the TS coordinate frequency is 74i cm^{-1}). More generally, this result may offer insight into why density functional theory characteristically underestimates barrier heights[11] and their associated reaction coordinate frequencies (i.e., an additional accounting of the exchange energy appears to be needed).

Last, Table 8 lists four of the bond parameters associated with the TS structure. As the balance of exchange is shifted from Hartree−Fock to Becke88, the TS structure moves from one that is E2-like to one that is more E1$_{cb}$-like. It appears, therefore, that it may be possible to locate anti elimination TS structures with the 6-31+G(d,p) basis set and any given functional by simply including an (undetermined) amount of Hartree−Fock exchange. These results offer further support for the currently preferred use of "hybrid" functionals.

Questions with respect to the apparently extreme basis set dependence of the anti elimination TS structure still need to be addressed. Why is possible to locate the TS structure with the aug-cc-pVDZ basis set but not the 6-31+G(d,p) basis set? Both bases are double split-valence and have additional polarization and diffuse functions. The key to the answer may lie with the fact that attempts to find anti elimination TS structures at the B-VWN5/cc-pVDZ level of theory failed. It would, therefore, appear that the diffuse functions of the aug-cc-pVDZ basis set are of critical importance. The augmentation in Dunning's basis set includes sets of spd and sp diffuse functions on second-row atoms and hydrogen atoms, respectively. The 6-31+G(d,p) basis set lacks the set of d diffuse functions on second-row atoms and possesses no diffuse functions whatsoever on hydrogen atoms. Searches with the 6-31++G(d,p) basis set also failed to locate TS structures (the second + sign signifies the inclusion of a set of s diffuse functions on hydrogen atoms). Hence, these negative finding are highly suggestive that, issues of correlation consistency aside, the basis set dependence resides with the necessity to include higher angular momentum diffuse functions (d- and/or p-type). While the exact nature of this dependency has as yet not been established, these higher angular momentum functions may confer a degree of directionality to the charge density which is essential in the description of complicated (inhomogeneous) electronic systems (e.g., the anti elimination TS structure).

Conclusions

As the above results and an ever growing body of literature demonstrate, DFT is capable of reproducing a number of thermochemical values. This optimism must be tempered by the fact that there is not a single functional or class of functionals that perform in a clearly superior fashion. Nevertheless, where density functional successes have occurred, they have typically been achieved at lesser expense than *ab initio* approaches. DFT seems to be at greatest variance with high-level *ab initio* calculations when it comes to the prediction of TS energies and structures, often yielding looser and more stable TS's. More distressing is the fact that density functional methods sometimes fail to locate TS's that are found by their more traditional

counterparts. The origin of this problem may reside in the large inhomogeneities in charge density that are characteristic of TS's and an inadequate description of the exchange interaction. Regardless, the ability of density functional methods to predict the nature of TS's demands a great deal more attention than it has received to date.

The present study has brought a number of relevant observations with respect to DFT to light: (1) Basis set saturation seems to occur much more quickly for density functional methods than for those of *ab initio* theory. Once the double split-valence level is reached, further improvement in basis set quality offers little in the way of structural or energetic improvement. (2) Noncorrelated functionals, especially those lacking Becke's gradient correction, are of questionable value. (3) Within a given class of functionals (e.g., locally correlated), there is only slight variation in structure and energy. This result is highly suggestive that improvement in density functional methods will only come with a fundamental change in the functionals themselves. (4) "Hybrid" functionals, which putatively offer a better accounting of the self-interaction exchange energy, seem to hold the most promise.

Acknowledgment. Support from the National Science Foundation, the donors of the Petroleum Research Fund, administered by the American Chemical Society, and the Minnesota Supercomputer Institute is gratefully acknowledged.

Supporting Information Available: Calculated aug-cc-pVDZ structures (*xyz* coordinates), energies, and imaginary frequencies for transition structures (25 pages). Ordering information is given on any current masthead page.

References and Notes

(1) (a) Gandler, J. R. *The Chemistry of Double-bonded Functional Groups;* Patai, S., Ed.; Wiley: New York, 1989; Vol. 2, Part I. (b) Reichardt, C. *Solvents and Solvent Effects in Organic Chemistry*, 2nd ed.; VCH: New York, 1988. (c) Bartsch, R. A.; Závada, J. *Chem. Rev.* **1980**, *80*, 453. (d) Alekserov, M. A.; Yufit, S. S.; Kucherov, V. F. *Russ. Chem. Rev.* **1978**, *47*, 134. (e) Saunders, W. H. *Acc. Chem. Res.* **1976**, *9*, 19. (f) Bartsch, R. A. *Acc. Chem. Res.* **1975**, *8*, 239. (g) Saunders, W. H.; Cockerill, A. F. *Mechanisms of Elimination Reactions*; Wiley: New York, 1973. (h) Bordwell, F. G. *Acc. Chem. Res.* **1972**, *5*, 374. (i) Wolfe, S. *Acc. Chem. Res*. **1972**, *5*, 102. (j) Bartsch, R. A.; Bunnett, J. F. *J. Am. Chem. Soc*. **1968**, *90*, 408. (k) Bunnett, J. F. *Angew. Chem., Int. Ed. Engl*. **1962**, *1*, 225. (l) Cram, D. J.; Greene, F. D.; DePuy, C. H. *J. Am. Chem. Soc*. **1956**, *78*, 790.

(2) (a) Gronert, S. *J. Am. Chem. Soc*. **1993**, *115*, 652. (b) Gronert, S. *J. Am. Chem. Soc*. **1992**, *114*, 2349. (c) Gronert, S. *J. Am. Chem. Soc*. **1991**, *113*, 6041. (d) Minato, T.; Yamabe, S. *J. Am. Chem. Soc*. **1988**, *110*, 4586. (e) Minato, T.; Yamabe, S. *J. Am. Chem. Soc*. **1985**, *107*, 4621. (f) Roy, M.; McMahon, T. B. *Can. J. Chem*. **1985**, *63*, 708. (g) Schleyer, P. v. R.; Kos, A. J. *Tetrahedron* **1983**, *39*, 1141. (h) Pross, A.; Shaik, S. S. *J. Am. Chem. Soc.* **1982**, *104*, 187. (i) Bach, R. D.; Badger, R. C.; Lang, T. J. *J. Am. Chem. Soc*. **1979**, *101*, 2845.

(3) (a) March, J. *Advanced Organic Chemistry*, 4th ed.; John Wiley and Sons: New York, 1992. (b) Lowry, T. H.; Richardson, K. S. *Mechanism and Theory in Organic Chemistry*, 3rd ed.; Harper and Row: New York, 1987.

(4) Parker, A. J.; Ruane, M.; Biale, G.; Winstein, S. *Tetrahedron Lett.* **1968**, *17*, 2113.

(5) (a) Sullivan, S. A.; Beauchamp, J. L. *J. Am. Chem. Soc*. **1976**, *98*, 1160. (b) Ridge, D. P.; Beauchamp, J. L. *J. Am. Chem. Soc*. **1974**, *96*, 3595. (c) Ridge, D. P.; Beauchamp, J. L. *J. Am. Chem. Soc*. **1974**, *96*, 637.

(6) (a) Rabasco, J. J.; Gronert, S.; Kass, S. R. *J. Am. Chem. Soc*. **1994**, *116*, 3133. (b) Rabasco, J. J.; Kass, S. R. *J. Org. Chem*. **1993**, *58*, 2633.

(7) Gronert, S.; Merrill, G. N.; Kass, S. R. *J. Org. Chem*. **1995**, *60*, 488.

(8) (a) Paar, R. G.; Yang, W. *Density-Functional Theory of Atoms and Molecules*; Oxford University Press: New York, 1989. (b) Jones, R. O.; Gunnarsson, O. *Rev. Mod. Phys.* **1989**, *61*, 689. (c) Dreizler, R. M.; Gross, E. K. U. *Density Functional Theory*; Springer: Berlin, 1990. (d) Ziegler, T. *Chem. Rev.* **1991**, *91*, 651. (e) Labanowski, J. K.; Andzelm, J. W., Eds. *Density Functional Methods in Chemistry*; Springer-Verlag: New York, 1991. (f) Bartolotti, L. J.; Flurchick, K. *Rev. Comput. Chem.* **1996**, *7*, 187. (g) St-Amant, A. *Rev. Comput. Chem.* **1996**, *7*, 217.

(9) Johnson, B. G.; Gill, P. M. W.; Pople, J. A. *J. Chem. Phys.* **1992**, *97*, 7846.

(10) Møller, C.; Plesset, M. S. *Phys. Rev.* **1934**, *46*, 618.

(11) (a) Baker, J.; Andzelm, J.; Muir, M.; Taylor, P. R. *Chem. Phys. Lett.* **1995**, *237*, 53. (b) Pederson, M. R. *Chem. Phys. Lett.* **1994**, *230*, 54. (c) Johnson, B. G.; Gonzales, C. A.; Gill, P. M. W.; Pople, J. A. *Chem. Phys. Lett.* **1994**, *221*, 100. (d) Stanton, R. V.; Merz, Jr., K. M. *J. Chem. Phys.* **1994**, *100*, 434. (e) Fan, L.; Ziegler, T. *J. Am. Chem. Soc.* **1992**, *114*, 10890.

(12) Bickelhaupt, F. M.; Baerends, E. J.; Nibbering, N. M. M.; Ziegler, T. *J. Am. Chem. Soc*. **1993**, *115*, 9160.

(13) While this manuscript was being reviewed we became aware of a related but distinct DFT study on the E2 and S_N2 reactions of $F^- + C_2H_5F$ + nHF. See: Bickelhaupt, F. M.; Baerends, E. J.; Nibbering, N. M. M. *Chem. Eur. J*. **1996**, *2*, 196. It is worth mentioning with regard to this paper and ref 12 that (a) as the authors note, the strength of a base in an elimination reaction (and substitution) will affect the geometry of the transition structure. (b) Diffuse functions are well-known to be needed to adequately describe anions (energies and geometries), and they were not included in the DZP basis set which was used to carry out the structural optimizations. The TZ2P basis set, which was used for energetic comparisons also does not include diffuse functions, but it is much more flexible. (c) Xα energetics are unreliable with regard to the $F^- + C_2H_5F$ system even when diffuse functions are included in double split-valence basis sets; see Tables 5 and 6 and ref 7. (d) Xα geometries are very different from *ab initio* and other, more sophisticated, DFT functionals; in short, they appear to be unreliable. (e) Finally, while the elimination reaction of F^- with C_2H_5F must lead to ethylene and FHF^- based upon thermodynamic grounds, there is no reason that the leaving group (F^-) and the protonated base (HF) need to interact in the transition state (this interaction is not seen with *ab initio* calculations or a wide variety of density functionals that include diffuse functions). These two species can find each other subsequently in the resulting long-lived ion−molecule complex. It is for this reason that cluster ions (e.g., FHF^-) are observed from both syn and anti 1,2 (and 1,4) eliminations. For further details about the stereochemistry of gas-phase elimination reactions, see refs 6 and 7.

(14) Hohenberg, P.; Kohn, W. *Phys. Rev. A* **1964**, *136*, 864.

(15) (a) Pople, J. A.; Gill, P. M. W.; Johnson, B. G. *Chem. Phys. Lett.* **1992**, *199*, 557. (b) Kohn, W.; Sham, L. J. *Phys. Rev. A* **1965**, *140*, 1133.

(16) Z_A and r_A are the charge of and distance to nucleus A, and r is the distance to an electron.

(17) Slater, J. C. *Quantum Theory of Molecules and Solids, Vol. 4: The Self-Consistent Field for Molecules and Solids*; McGraw-Hill: New York, 1974.

(18) Vosko, S. H.; Wilk, L.; Nusair, M. *Can. J. Phy*. **1980**, *58*, 1200.

(19) Becke, A. D. *Phys. Rev. A* **1988**, *38*, 3098.

(20) Perdew, J. P. *Phys. Rev. Lett.* **1985**, *55*, 1665.

(21) Lee, C.; Yang, W.; Paar, R. G. *Phys. Rev. B* **1988**, *37*, 785. As has been noted by Becke,[37] the LYP functional suffers from an inability to reproduce the homogeneous electron gas limit exactly and treat opposite- and parallel-spin correlations uniquely.

(22) Perdew, J. P. *Phys. Rev. B* **1986**, *33*, 8822. Like LYP, the PW91 functional is not free of flaws as it has self-interaction.

(23) Perdew, J. P.; Wang, Y. *Phys. Rev. B* **1992**, *45*, 13244.

(24) (a) Hehre, W. J.; Ditchfield, R.; Pople, J. A. *J. Chem. Phys.* **1972**, *56*, 2257. (b) Hariharan, P. C.; Pople, J. A. *Theor. Chim. Acta* **1973**, *28*, 213. (c) Gordon, M. S. *Chem. Phys. Lett.* **1980**, *76*, 163. (d) Frisch, M. J.; Pople, J. A.; Binkley, J. S. *J. Chem. Phys.* **1984**, *80*, 3265. (e) Clark, T.; Chandrasekhar, J.; Spitznagel, G. W.; Schleyer, P. v. R. *J. Comput. Chem.* **1983**, *4*, 294. (f) Frisch, M. J.; Head-Gordon, M.; Pople, J. A. *Chem. Phys. Lett.* **1990**, *166*, 281.

(25) (a) Dunning, Jr., T. H. *J. Chem. Phys.* **1989**, *90*, 1007. (b) Kendall, R. A.; Dunning, Jr., T. H.; Harrison, R. J. *J. Chem. Phys.* **1992**, *96*, 6796.

(26) Perdew, J. P.; Zunger, A. *Phys. Rev B* **1981**, *23*, 5048.

(27) It should be noted that the original "hybrid" functional of Becke made use of the nonlocal correlation functional of Perdew and Wang.[23] Becke, A. D. *J. Chem. Phys.* **1993**, *98*, 5648. The Becke3-LYP and Becke3-P86 functional forms are Gaussian 92/DFT and Gaussian 94 implementations.

(28) Curtiss, L. A.; Raghavachari, K.; Trucks, G. W.; Pople, J. A. *J. Chem. Phys*. **1991**, *94*, 7221.

(29) Gronert, S. *J. Am. Chem. Soc*. **1993**, *115*, 10258.

(30) These calculations do not use the counterpoise approach described in the original publication.[29] As this correction lowers the G2+ energy of fluoride by 2.0 kcal/mol, its inclusion would add +2.0 kcal/mol to all of the G2+ barriers. The reaction enthalpies for eqs 7, 9, and 10 would be 370.2, −31.1, and 43.2 kcal/mol, respectively. The DFT energies for F^- are effected less by the counterpoise correction (∼0.5 kcal/mol) and thus the difference in all of the reported barriers would increase by approximately 1.5 kcal/mol. For further details on how to treat small anions, see: Gronert, S. *Chem. Phys. Lett*. **1996**, *252*, 415.

(31) (a) Gaussian 94, Revisions A and B, Frisch, M. J.; Trucks, G. W.; Schlegel, H. B.; Gill, P. M. W.; Johnson, B. G.; Robb, M. A.; Cheeseman, J. R.; Keith, T.; Petersson, G. A.; Montgomery, J. A.; Raghavachari, K.; Al-Laham, M. A.; Zakrzewski, V. G.; Ortiz, J. V.; Foresman, J. B.;

Cioslowski, J.; Stefanov, B. B.; Nanayakkara, A.; Challacombe, M.; Peng, C. Y.; Ayala, P. Y.; Chen, W.; Wong, M. W.; Andres, J. L.; Replogle, E. S.; Gomperts, R.; Martin, R. L.; Fox, D. J.; Binkley, J. S.; Defrees, D. J.; Baker, J.; Stewart, J. P.; Head-Gordon, M.; Gonzalez, C.; Pople, J. A. Gaussian, Inc.: Pittsburgh PA, 1995. (b) Frisch, M. J.; Trucks, G. W.; Schlegel, H. B.; Gill, P. M. W.; Johnson, B. G.; Wong, M. W.; Foresman, J. R.; Robb, M. A.; Head-Gordon, M.; Replogle, E. S.; Gomperts, R.; Andres, J. L.; Raghavachari, K.; Binkley, J. S.; Gonzales, C. A.; Martin, R. C.; Fox, D. J.; Defrees, D. J.; Baker, J.; Stewart, J. J. P.; Pople, J. A. GAUSSIAN-92/DFT; Gaussian Inc.: Pittsburgh, PA, 1993.

(32) All thermodynamic data, unless otherwise noted, come from: Lias, S. G.; Bartmess, J. E.; Liebman, J. F.; Holmes, J. L.; Levin, R. D.; Mallard, W. G. *J. Phy. Chem. Ref. Data* **1988**, *17*, Supplement 1, or the slightly updated form available on a personal computer, *NIST Negative Ion Energetics Database* (Version 3.00, 1993); NIST Standard Reference Database 19B.

(33) Only three of these reactions are independent of each other (i.e., (8) − (9) = (10)).

(34) Wenthold, P. G.; Squires, R. R. *J. Phys. Chem.* **1995**, *99*, 2002.

(35) For example, see: Hertwig, R. H.; Koch, W. *J. Comput. Chem.* **1995**, *16*, 576.

(36) (a) Kebarle, P. *Annu. Rev. Phys. Chem.* **1977**, *28*, 445. (b) DePuy, C. H.; Bierbaum, V. M. In *Structure/Reactivity and Thermochemistry of Ions*; Ausloos, P., Lias, S. G., Eds.; D. Reidel: Dordrecht, 1987; p 293.

(37) (a) Oliphant, N.; Bartlett, R. J. *J. Chem. Phys.* **1994**, *100*, 6550. (b) Johnson, B. G.; Gill, P. M. W.; Pople, J. A. *J. Chem. Phys.* **1993**, *98*, 5612. (c) Andzelm, J.; Wimmer, E. J. *Chem. Phys.* **1992**, *96*, 1280.

(38) Becke, A. D. *J. Chem. Phys.* **1996**, *104*, 1040.